

Project: 1034

Project title: JPI-Climate project InterDec

Project lead: Dr. Daniela Matei

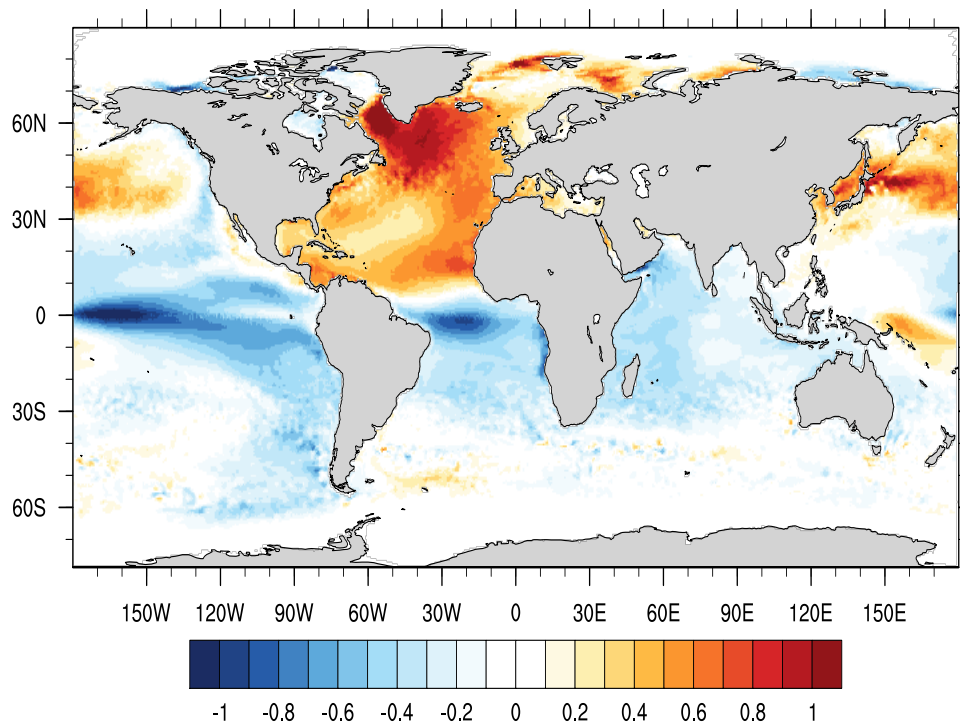
PIs: Dr. Daniela Matei, Dr. Jürgen Bader, Dr. Katja Lohmann, Dr. Elisa Manzini.

Achievements in 2018:

Interbasin linkages

Regarding the interbasin linkages to be investigated within InterDec, the DCPD sensitivity experiments prescribing the sea surface temperature (SST) pattern related to the Atlantic Multidecadal Variability (AMV) are of high interest to InterDec, especially those applying the relatively high-resolution T255/TP04 configuration, as conducted within H2020 project PRIMAVERA. Performing the latter in sufficient ensemble size, is, however, a computationally expensive exercise, which has been supported by InterDec.

An interesting result of the experiments is that the SST composite (AMV+ minus AMV-) averaged over five ensemble members does not only show large anomalies in the North Atlantic (where the SST is



prescribed), but also in the tropical and North Pacific (Fig. 1). In general, one would expect relatively small anomalies outside the North Atlantic due to internal variability being smoothed out when averaging over a large ensemble size. The SST anomalies in the Pacific resemble the El Niño – Southern Oscillation as well as the Interdecadal Pacific Variability (IPV) pattern, indicating that the large-scale climate modes like AMV and IPV influence each other.

Figure 1: Composite of SST between experiments prescribing a positive and negative phase of the AMV, respectively averaged over five ensemble members. Courtesy of Katja Lohmann

Nonlinear Response of the Stratosphere and the North Atlantic-European Climate to Global Warming

The response of the Northern winter atmospheric circulation for two consecutive global warming periods of 2K is examined in a grand ensemble (68 members) of idealized CO₂ increase experiments performed with the same climate model. The comparison of the atmospheric responses for the two periods shows remarkable differences, indicating the nonlinearity of the response (Fig. 2). The stratospheric vortex response shifts from an easterly wind change for the first 2K to a westerly wind change for the second 2K (Fig. 2a,b) and the North Atlantic storm track shifts poleward only in the second period (Fig. 2d,e), when also the pressure at sea level shows a pronounced see-saw pattern (Fig. 2g,h). The nonlinear signature of the atmospheric and surface responses is reminiscent of the positive phase of the annular mode of variability (Fig. 2c,f and i). Among the factors leading to the nonlinear response, we find that differences in Arctic sea ice changes between the two periods can act to trigger the atmospheric nonlinear response. Thereafter, stratosphere-troposphere coupling appear to provide for the persistence of this nonlinearity throughout the winter.

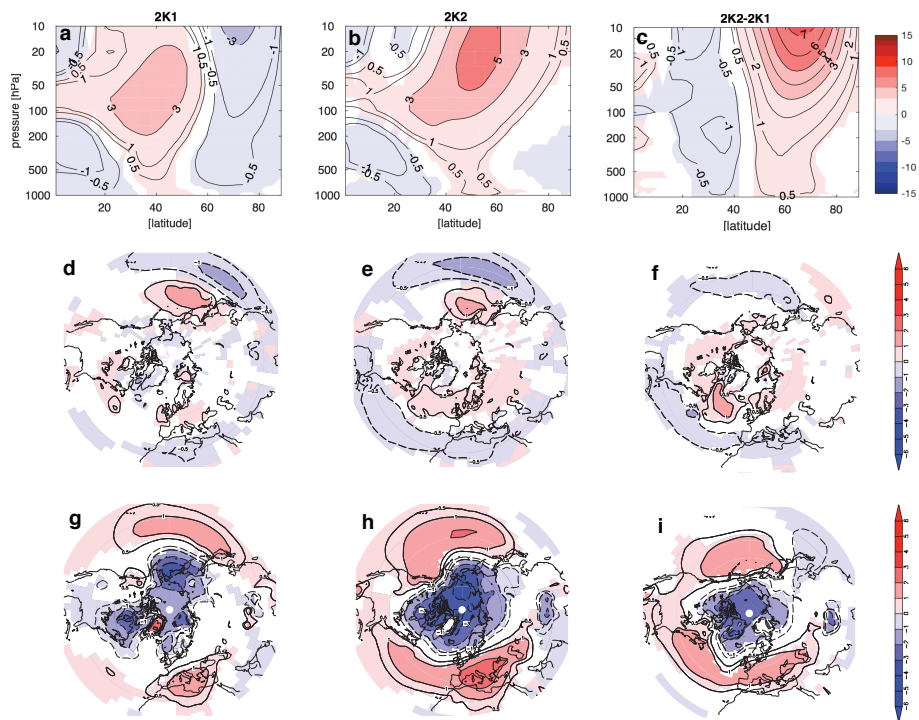


Figure 2. January response of zonal mean zonal wind (ms^{-1}) to (a) the first and (b) the second 2K of global warming; and (c) their difference. (d-f) Same as Figures (a-c) but shown is near surface (10 m) zonal wind (ms^{-1}). (g-i) Same as Figures (a-c) but shown is pressure at sea level (hPa) Contours: (a-b) ± 0.5 , ± 1 and then each 2 ms^{-1} ; (c) ± 0.5 , ± 1 and then each 1 ms^{-1} ; (d-f) ± 0.5 , ± 1 and then each 1 ms^{-1} ; (g-i) ± 0.5 , ± 1 and then each 1 hPa . Colored areas indicate significance with $p < 0.05$.

Reference

Manzini, E., A. Yu. Karpechko, and L. Kornbluh (2018) *Nonlinear Response of the Stratosphere and the North Atlantic-European Climate to Global Warming*, Geophysical Research Letters DOI:10.1029/2018GL077826.

Coordinated Arctic sea-ice sensitivity experiments

The InterDec coordinated Arctic sea-ice sensitivity experiments have been designed in Dec. 2017 together with the partner group from the University of Niigata. Accordingly, two sea ice forcing fields are derived from the climatological monthly means of 10 years in which the observational November sea-ice concentrations (SICs) over the Barents-Kara Sea are lowest or highest considering the time period July 1981 to June 2016 (Fig.3). For these computations the SIC and sea-surface temperature (SST) data set “COBE” was chosen, because (1) the data are available in daily resolution and (2) the SICs and SSTs are adjusted in a physically consistent way. Until now two institutes (Niigata University and MPI-M) have carried out the coordinated experiments (employing the ECHAM6 and AFES AGCMs), with two more partners about to be joining the efforts soon.

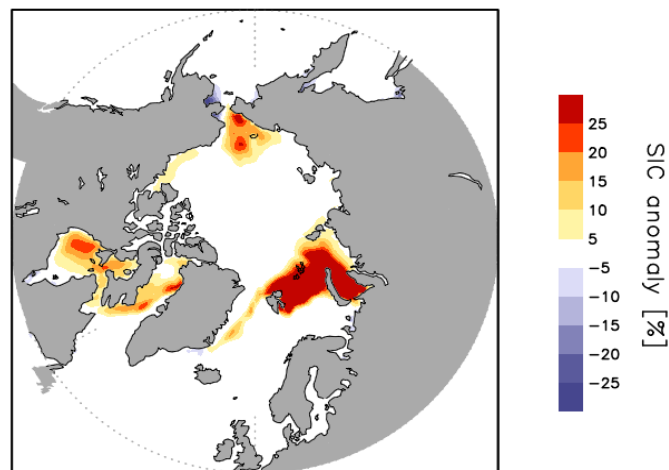


Figure 3: Difference in the Arctic low and high sea-ice concentrations forcing fields. Here shown for November.

InterDec BKS sea ice experiment protocol time-slice setup

- 100 yrs integration (after at least 10 yrs spin-up)
- Boundary conditions: COBE-SSTv2 (daily SIC and SST)
SST: clim of 01JUL1981-30JUN2016
SH sea ice: clim of 01JUL1981-30JUN2016
NH sea ice: 10 yrs avgs based on Nov BKS (30-90E, 65-85N)
High ice (01JUL-30JUN, 82/83, 88/89, 90/91, 91/92, 92/93, 93/94, 94/95, 97/98, 98/99, 02/03)
Low ice (01JUL-30JUN, 96/97, 00/01, 07/08, 08/09, 09/10, 10/11, 11/12, 12/13, 13/14, 15/16)

Other external conditions

- 3-D O3 CMIP6 climatology over 01JAN-31DEC 1981-2014
- CO₂, CH₄, N₂O, and CFC annual mean global average over 1981-2014 based on CMIP6
- Stratospheric H₂O, prescribed value in each model
- Orbital forcing (3 parameters) defined as 1998 value (the mid-year of the period of 1981-2015) if not fixed in the model

The geopotential height response to the reduction in Arctic sea ice shows an equivalent barotropic structure. A height decrease in the Pacific sector and around the British Isles and an increase in the region of the Ural Mountain region (Fig. 4 left). The near-surface temperature response shows some cooling over eastern Siberia and warming over Eastern Europe (Fig. 4 right). Further investigations are necessary whether the geopotential height changes over the Urals and the continental temperature changes over Europe and Asia are associated with changes in the atmospheric blocking frequency in the region of the Urals. Additional analysis shows also that the stratosphere might be involved in the Arctic sea-ice response via sea-ice induced stratospheric changes that propagate downwards into the troposphere.

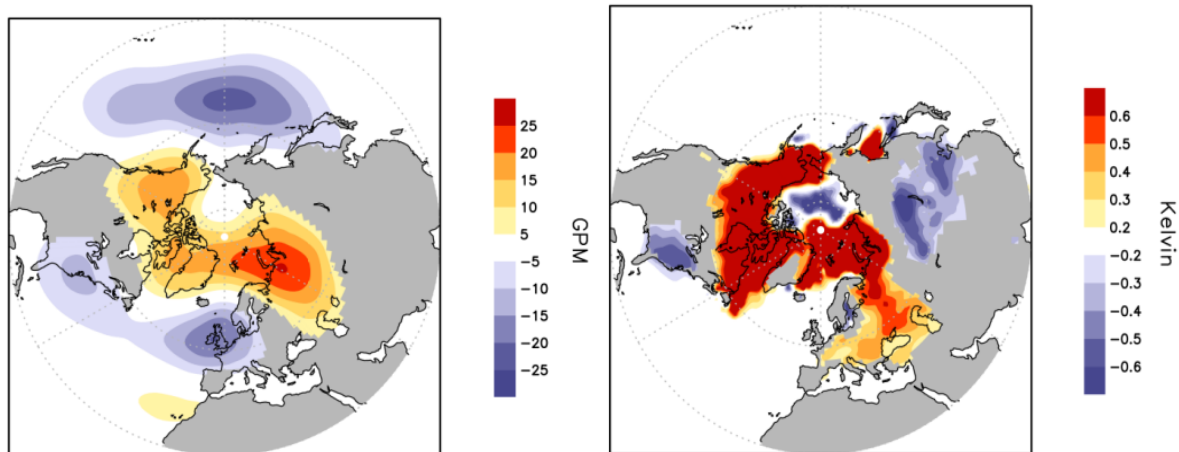


Figure 4: 500 hPa geopotential height (left) and near surface temperature response (low minus high Arctic SICs).

To test the role of the background state and the role of tropical versus extra-tropical forcing four additional experiments with ECHAM6 are currently performed: positive and negative NAO-like (background state) are induced by a warm/cold Indian Ocean. Under these new different background states the sea-ice response is investigated. The additional experiments indicate that the sea-ice response might substantially dependent on the background state of the atmosphere. Fig. 5 left shows the 500 hPa geopotential height response in March for the control climate and Fig. 5 right for the positive NAO-like state.

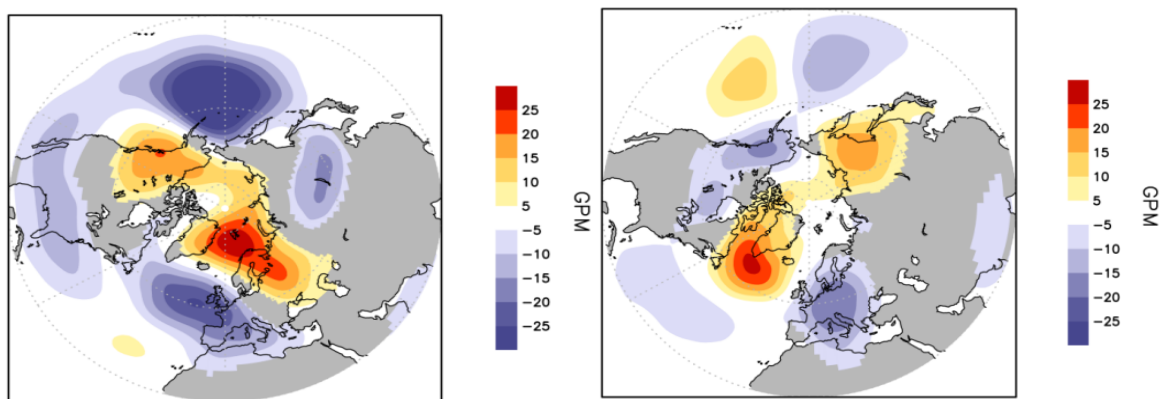


Figure 5: 500 hPa GPH response in March for unmodified background state (left) and positive NAO-like background state (right) .

The role of Ural blocking in driving the Warm Arctic Cold Siberia (WACS) pattern

Atmospheric blocking is linked to high impact weather extremes in mid-latitudes. Arctic Amplification and the consequent weakening of the meridional temperature gradient in mid-latitudes have been seen as the cause of a weaker and more meandering mid-latitude westerly jet that favors blocking. However, the evidence for a recent increase in blocking activity across the Northern Hemisphere and a wavier jet has been disputed. In particular Ural Blocking (UB) represents an important part in the spectrum of atmospheric variability over Eurasia and it has been envisaged as the driving mechanism of the recent cooling over central Asia (CAS) and warming over the Barents-Kara Seas (BKS), which combined manifest as the Warm Arctic Cold Siberia (WACS) pattern (Fig. 6a). If so then the recent cooling trend over mid-latitude Eurasia should be expected to be accompanied by an upward trend

in blocking. To further investigate this hypothesis, we used ERA-Interim data and we employed the PV- θ blocking index as a diagnostic to investigate trends in blocking activity in recent decades. We identified a statistically significant upward trend in UB that coincided with the recent increasing trend in cold extremes over central Asia (Fig. 6c). The longitudinal and latitudinal position of blocking determines the exact location of the induced cooling and warming. UBs are particularly efficient in inducing an atmospheric circulation that results in cooling (warming) over the CAS (BKS) that markedly projects on the WACS pattern (Fig. 6b).

The WACS pattern emerges as the second EOF of surface temperature variability over Eurasia (Fig. 6d). We defined a WACS index (WACSI) as the difference of area-averaged DJF-mean T2m over the BKS (30-80°E, 75-85°N) minus T2m averaged over central Asia (70-110°E, 50-60°N). The two areas are delineated by the boxes in Fig. 6f while the WACSI timeseries is shown in Fig. 6e. The correlation between the WACSI and PC2 timeseries is 0.9, which suggests that PC2 timeseries can be used as a proxy of the temporal evolution of the WACS pattern. The interannual variability of the WACS intensity and its trends match that of UB activity. Nearly every peak in WACSI/PC2 occurs in association with high UB activity. Evidently, after 2000 there is an upward trend of the WACSI/PC2 while the overwhelming majority of high-WACSI/PC2 winters occurred after 2005, reflecting the more frequent occurrence of colder (warmer) winters over CAS (BKS). WACS is particularly linked to blocking that occurs within the latitude band 60-65°N, hereafter UB (Fig. 6f). Higher latitude Arctic blocking is strongly associated with an annular-like mode (first EOF), but is less relevant to the WACS, as it induces a warming-over-cooling dipole that is shifted polewards, compared to the WACS. Very high-latitude blocking can also induce cold spells over high latitude Eurasia but the WACS dipole manifests itself better through UB occurrence.

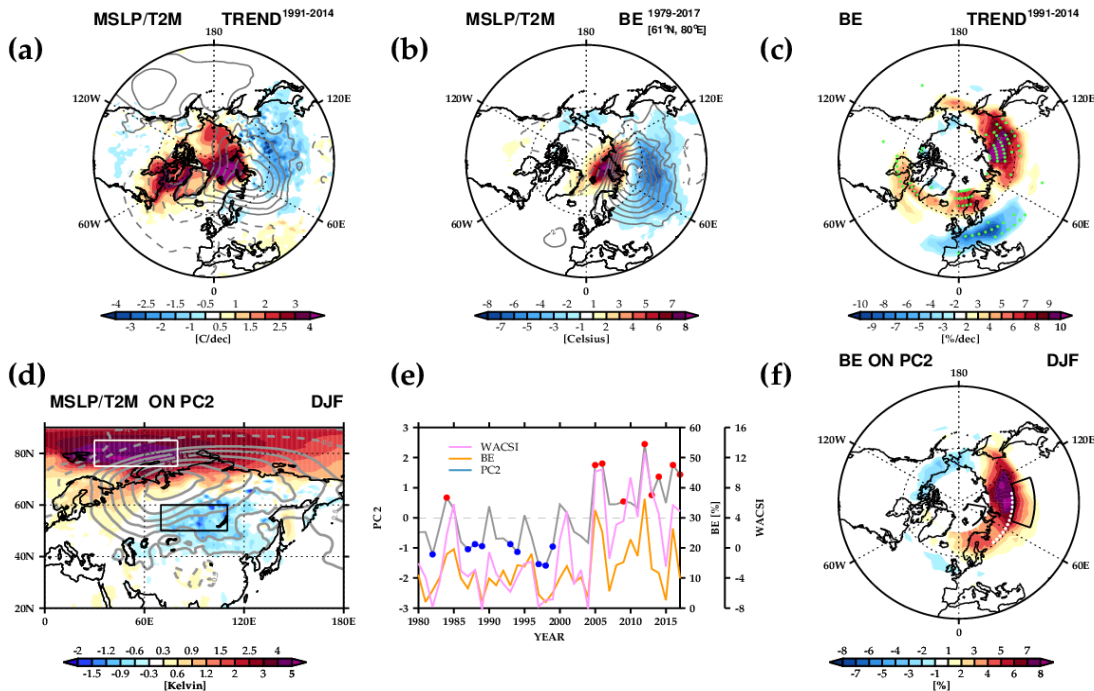


Figure 6. (a) Linear trend of DJF-mean MSLP (solid contours) and T2M (color shades) during the period 1991-2014. (b) Composite mean departures of MSLP (contours; in hPa) and T2M (color shades; in Celsius) from the daily seasonal cycle only for days when BE is identified during the period 1979-2017 at 80°E, 61°N. The contour interval is 2 hPa, solid (dashed) lines denote positive (negative) trends while the zero contour is suppressed. (c) Linear trend of DJF-mean BE

frequency (% per decade) during 1991-2014. Green dots mark grid-points where the trends are statistically significant at the 95 % level. (d) Regression of DJF-mean MSLP (color shades) and T2M (contours) on the second normalized Principal Component (PC2). The contour interval is 0.5 hPa, solid (dashed) lines denote positive (negative) values while the zero contour is suppressed. (e) Interannual evolution of normalized PC2 (grey), DJF-mean blocking frequency (orange) averaged over the sector 40-100°E, 61°N and WACS Index (WACSI; purple). Red (blue) dots mark the winter belonging to the upper (lower) quartile of PC2. (f) Regression of DJF-mean blocking frequency on the normalized PC2. The dots delineate the sector that blocking frequency is averaged (orange lines in e). Black boxes delineate the regions in which the WACSI is calculated: BKS (30-80°E, 75-85°N) and CAS (70-110°E, 50-60°N). From Tyrllis et al., 2018.

We analyzed daily fields and we concluded that UB sets the pace of the WACS on short timescales. The anticyclonic circulation over the Urals induces warm advection over the BKS and cold surges over central Asia and the surface temperature anomalies peak 3-5 days after the UB onset (Fig. 7ab). The Arctic waters warm at a slower pace, while sea ice melting peaks around 10 days after the blocking onset and persist for up to 3 weeks (Fig. 7cd). The fast building and decay of the anomalous downward surface fluxes, following the pace of surface air temperature anomalies, suggest that the Cryospheric changes are slave to the atmosphere (Fig. 7ef).

Winters with more frequent UB favor the emergence of the WACS signal in seasonal means. Thus, the interannual variability of BKS and CAS T2m is strongly linked to UB and during winters with high (low) UB activity BKS warming and CAS cooling are enhanced (weakened). Over the BKS the UB induced warming is embedded in the strong recent Arctic warming that dominated trends (Fig. 7g). In mid-latitude Eurasia the internal atmospheric variability associated with UB emerges as the dominant process and appears to be key in setting the pace in the interannual variability of central Asia temperature anomalies and its trend. The recent negative trend over CAS is reduced by almost 2/3 when the days of winter UB are removed (Fig. 7h).

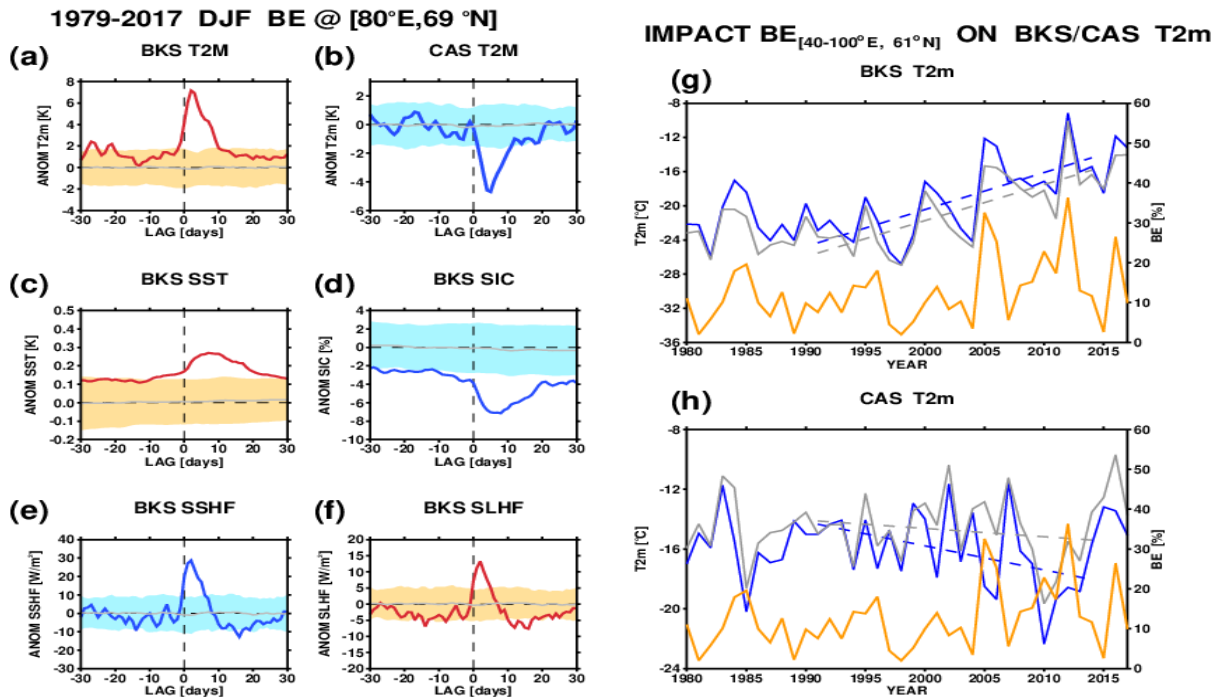


Figure 7. (a,b) Daily evolution of composite T2m anomalies relative to the onset of UB occurring at 60°E, 65°N. Anomalies are averaged over the BKS (30-80°E, 75-85°N) and CAS (60-100°E, 50-60°N). Only DJF onset days during the period 1979-2017 are included. (c-f) As in Fig. 7a,b but for

composite anomalies of Sea Ice Cover (SIC), SST, Surface Sensible Heat Fluxes (SSHF) and Surface Latent Heat Fluxes (SLHF) averaged over the box region (20-60°E, 70-80°N). The statistical significance of the area-averaged anomalies is assessed with the aid of a Monte Carlo style method. In areas where the curves lie outside the shaded regions, the anomalies are statistically significant at the 95% level. (f) Interannual evolution of the DJF-mean temperature averaged over the BKS (40-90°E, 75-85°N) for all DJF days (blue), only for days without blocking detected over the sector 40-100°E, 61°N (grey) and DJF mean blocking episode frequency averaged over the same sector (orange). The linear fit during the period 1991-2014 is also depicted by the dashed lines and the corresponding trend in °C per decade is shown in the legend. (g) As in Fig. 7f, but for T2m averaged over the CAS (60-100°E, 50-60°N). From Tyrllis et al., 2018.